Synthesis and characterization of nanoscale composite particles formed by 2D layers of Cu-Fe sulfide and Mg-based hydroxide

Yuri L. Mikhlin[a], Roman V. Borisov[a,c], Sergey A. Vorobyev[a], Yevgeny V. Tomashevich[a], Alexander S. Romanchenko[a], Maxim N. Likhatski[a], Anton A. Karacharov[a], Oleg A. Bayukov[b], Yuriy V. Knyazev[b], Dmitriy A. Velikanov[b], Sergey M. Zharkov[b,c], Alexander S. Krylov[b], Svetlana N. Krylova[b], Ivan V. Nemtsev[b,c,d]*

[a] Institute of Chemistry and Chemical Technology, Krasnoyarsk Science Center of the Siberian Branch of the Russian Academy of sciences, Akademgorodok, 50/24, Krasnoyarsk, 660036, Russia

[b] Kirensky Institute of Physics, Krasnoyarsk Science Center of the Siberian Branch of the Russian Academy of sciences, Akademgorodok 50/38, Krasnoyarsk, 660036, Russia

[c] Siberian Federal University, Svobodny av. 79, Krasnoyarsk, 660041, Russia

[d] Federal Research Center "Krasnoyarsk Science Center of the Siberian Branch of the Russian Academy of sciences", Akademgorodok, 50, Krasnoyarsk, 660036, Russia

KEYWORDS: two-dimensional materials, composite, sulfide, hydroxide, valleriite, hydrothermal synthesis, colloids, X-ray photoelectron spectroscopy, Mössbauer spectroscopy, UV-vis-NIR, zeta potential.

ABSTRACT. Two-dimensional phenomena are attracting enormous interest at present and the search for novel 2D materials is very challenging. We propose here the layered material valleriite composed of altering atomic sheets of Cu-Fe sulfide and Mg-based hydroxide synthesized via a simple hydrothermal pathway as particles of 50-200 nm in the lateral size and 10-20 nm thick. The solid products and aqueous colloids prepared with various precursor ratios were examined using XRD, TEM, EDS, X-ray photoelectron spectroscopy (XPS), reflection electron energy loss spectroscopy (REELS), Raman, Mössbauer, UV-vis-NIR spectroscopies, magnetic, dynamic light scattering, zeta potential measurements. The material properties are largely determined by the narrow-gap (less than 0.5 eV) sulfide layers containing Cu^{+} and Fe^{3+} cations, monosulfide and minor polysulfide anions but are strongly affected by the hydroxide counterparts. Particularly, Fe distribution between sulfide (55-90%) and magnesium hydroxide layers is controlled through insertion of Al into the hydroxide part and by Cr and Co dopants entering both layers. Room-temperature Mössbauer signals of paramagnetic Fe^{3+} transformed to several Zeeman sextets with hyperfine magnetic fields up to 500 kOe in the sulfide layers at 4 K. Paramagnetic or more complicated characters were observed for valleriites with higher and lower Fe concentrations in hydroxide sheets, respectively. Valleriite colloids showed negative zeta potentials, suggesting negative electric charging of the hydroxide sheets, and optical absorption maxima between 500 nm and 700 nm, also depended on the Fe distribution. The last features observed also in the REELS spectra may be due to localized surface plasmon or, more likely, quasi-static dielectric resonance. The tunable composition, electronic, magnetic, optic and surface properties highlight valleriites as a rich platform for novel 2D composites promising for numerous applications.

1. Introduction

Two-dimensional (2D) materials attract much attention nowadays[1-13] owing to the large specific surface area and a wide spectrum of unique physical and (electro)chemical properties, which are of vivid interest for electronics, spintronics, energetics, sensors, photonics, catalysis, biomedical applications, and other areas. Many efforts have been made in recent years to manufacture and explore such materials beyond graphene as transition metal dichalcogenides, chalcogenides and ternary metal dichalcogenides,[11-16] constructed by two-dimensional sheets stacked mainly by van der Waals (vdW) forces. For example, MoS_2 and related substances having metallic conductivity are rather inert because of a low density of active centers and should be modified for many applications, while other metal chalcogenides incline to undesirable oxidation and corrosion.[11-19] A variety of electronic, magnetic, optical properties of Mo and W dichalcogenides, as well as MXenes with $Ti_3C_2T_x$ as a typical representative (T_x is the surface terminal groups O, OH, S, F), is limited by the metal nature. Consequently, the search for novel two-dimensional systems with requested characteristics is a very challenging task.

We report here a simple hydrothermal synthetic route to 2D composites constructed by alternating atomic sulfide layers close to $CuFeS_2$ composition and magnesium hydroxide-based sheets and their main characteristics. The natural prototype of this material is mineral valleriite[20-30] that remains insufficiently explored and its ores are not involved in commercial processing, despite the high content of heavy and precious metals.[28,29] The minerals usually contain Al and Fe cations partially substituting Mg in the brucite-like hydroxide layers, whereas sulfide layers are often depleted in Fe. For instance, Hughes et al.[30] have reported the composition of synthetic valleriites ranged from $[CuFeS_2]\cdot 1.67[Mg_{0.70}Al_{0.30}(OH)_2]$ to $[Cu_{1.30}Fe_{0.70}S_2]\cdot 1.35[Mg_{0.74}Al_{0.26}(OH)_2]$. Minerals of the valleriite group[31-34] can have prevalent iron in hydroxide layers (ferrovalleriite),[31,32] or chromium instead of iron in hydroxide and sulfide sheets.[33] These findings imply that such synthetic systems should be stable and their chemical composition could be widely varied and adjusted on demand.

Valleriite has been established[20,24,25,30] to crystallize in a hexagonal lattice with the sulfide sublattice being rhombohedral (space group $R\bar{3}m$ with hexagonal axes a = 0.3792 nm and c = 0.341 nm) and the hydroxide one having hexagonal lattice (space group $P\bar{3}m1$, a = 0.307 nm and c = 1.137 nm). Two atomic S layers form tetrahedral sites occupied, probably statistically, by Cu^+ and Fe^{3+} cations, whereas metals are in octahedral coordination with OH^- anions in the hydroxide part (Figure 1). Al^{3+} cations located in Mg^{2+} sites have been suggested to induce a positive electric charge of the brucite-type layer, so the sulfide sheets are charged negatively, and the quasi-monoatomic layers to be stacked by the opposite electric charges,[30] in contrast to more common vdW materials. Iron is thought to occur as preferential Fe^{3+}-S centers but Fe^{2+}-S, Fe^{3+}-OH and Fe^{2+}-OH species to exist too, as derived from ^{57}Fe Mössbauer spectra at room temperature.[26,35-37] Recently, we acquired X-ray absorption spectra together with Mössbauer and magnetic measurements for natural valleriite samples[38,39] and found that the central Mössbauer signal of paramagnetic iron transforms to a series of Zeeman sextets owing to internal local magnetic fields arising below 70 K but antiferromagnetic ordering characteristic of bulk chalcopyrite $CuFeS_2$ and other Cu-Fe sulfides[40] was absent. Exact nature of Fe species, as well as many properties of natural valleriites, remain uncertain due to complex composition of the mineral assemblages.

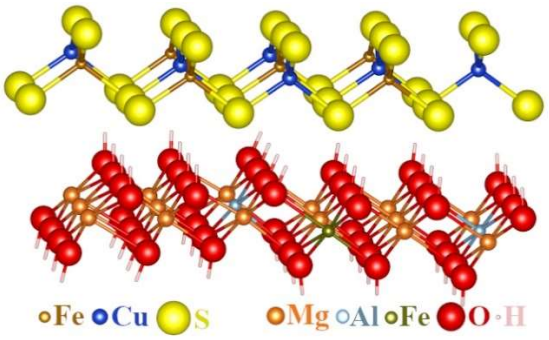

Figure 1. Scheme of atomic structures of Cu-Fe sulfide and $(Mg,Fe,Al)(OH)_2$ sheets in valleriite (slightly tilted for better view).

The attempts to synthesize valleriite via thermal sintering or hydrothermal routes have been undertaken[30,35-37,41,42] but mixtures of valleriite with chalcopyrite, magnetite and other by-products have been obtained. It should be noted that a number of layered composites of lithium-based and some other hydroxides and iron selenides $(Li_{1-x}Fe_x)(OH)\cdot FeSe$,[43-47] $[(Fe,Al)(OH)_2][FeSe]_{1.2}$,[48] iron sulfides $[(Li_{0.8}Fe_{0.2})OH]Fe(S_{1-x}Se_x)$,[49] $(Na_xFe_{1-x})(OH)FeS$[50] and similar[51] have been prepared and studied with focus on their superconductivity (critical temperature T_c up to 40 K). However, the compounds with alkaline metal hydroxides tend to hydrolysis hindering their exploration and wider exploitation.

The aims of the current study were to develop a pathway for production of pure valleriites, including colloidal solutions, to estimate effects of the material modification (with Al, Si, Cr, Co, rare earth metals), and to elucidate their basic characteristics. One more target was to outline the promises and problems of spectroscopic techniques (XPS, Mössbauer, UV-vis-NIR, Raman) for characterization of these uncommon materials. The results highlight the valleriite family, $m(Cu,Fe)S_2$ $n(Mg,Al,Fe)(OH)_2$ as a new platform for multifunctional two-dimensional composites with special and controllable properties for a variety of applications and some intriguing features, requiring further investigation.

2. Experimental section

2.1. Materials and synthetic procedures

Analytical grade iron (II) sulfate $FeSO_4\cdot 7H_2O$, copper sulfate $CuSO_4\cdot 5H_2O$, sodium sulfide $Na_2S\cdot 9H_2O$, magnesium sulfate $MgSO_4\cdot 7H_2O$, aluminum sulfate $Al_2(SO_4)_3\cdot 18H_2O$, cobalt(II) chloride $CoCl_2\cdot 6H_2O$, chromium(III) chloride $CrCl_3\cdot 6H_2O$, lanthanum(III) chloride $LaCl_3\cdot 7H_2O$, gadolinium(III) nitrate $Gd(NO_3)_3\cdot 5H_2O$ and aqueous ammonia were used without further purification. Deionized water (Millipore Milli-Q grade) was utilized to prepare the reagent solutions, to wash the precipitates, etc. In a typical procedure, pre-determined quantities of Fe and Cu sulfates (e.g., 0.556 g and 0.50 g, respectively) were dissolved in a small water volume and freshly prepared 20% solution of Na_2S was slowly added under agitation, producing black precipitate of metal sulfides. Gelatinous sediments of magnesium hydroxide or its mixture with aluminum hydroxide were obtained by adding 25% aqueous ammonia to aqueous solutions of Mg and Al sulfates. Then, this dispersion was transferred to the glass with Fe and Cu sulfides, pH was adjusted to 10-11 with aqueous ammonia, and the mixture was loaded into an in-home made stainless steel with Teflon liner autoclave[52] (Figure S1). The vessel (32 cm^3) was purged with Ar and sealed. The autoclave was rotated (8 rpm) at room temperature for about 1 h and then heated to 160 ^oC using air thermostat. After the heating

(2 h to 100 h), the autoclave was cooled in air, and solid products were separated using centrifugation (CR4000, Centurion Scientific, UK) at 4000 Hz for 15 min. The precipitate was washed 4-5 times via re-dispersion in water and centrifugation. The residue was stored as a wet paste and dried in air at room temperature before examination; the samples washed and dried with acetone or ethanol were found to be more oxidized. So, the process was performed using a large, 2-to-10-fold excess of sulfide anions relative to the $CuFeS_2$ stoichiometry, with excessive reagents rejected upon the centrifugation and washing. Totally, more than 50 specimens were successfully manufactured, as confirmed using XRD and XPS. Table 1 shows designations and the synthesis conditions for valleriite samples selected to present in this paper; the letters (a)-(i) are used to mark the specified samples throughout the article.

Table 1. Designations, atomic proportions of precursors, and time of heating under hydrothermal conditions (160 ºC) for selected valleriite samples

Sample	Atomic proportions of precursors						Time
index	Fe	Cu	S	Mg	Al	Dopant	(h)
a	2	1	10	2	-	-	33
b	2	1	14	2	2	-	33
c	2	2	15	1.5	1.5	-	50
d	2	2	14	2	0.5	-	25
e	1.8	2	14.8	1.5	1	Cr 0.2	50
f	1.5	2	14.8	1.5	1	Cr 0.5	50
g	1.8	2	14.8	1.5	1	Co 0.2	50
h	1.8	2	14.8	1.5	1	La 0.2	50
i	2	2	14	2	0.5	Si 1.0	32

To produce colloidal solutions, the residue (approximately 0.01 g) was dispersed in 50 mL of aqueous 2 mM sodium dodecyl sulfate (SDS) solution (Merck) with ultrasonic treatment (22 kHz, 15 W/cm^2, 3 min) with a Volna-M source (Center of ultrasound technologies, Russia). Colored supernatants (sols) spontaneously formed in some cases during centrifugation were diluted with water before examination.

2.2. Characterization

X-ray powder diffraction patterns were obtained from air-dried powders using a PANalytical X'Pert Pro diffractometer with Cu Kα radiation.

Transmission electron microscopy (TEM) images, energy dispersive X-ray analysis (EDS) and selected area electron diffraction (SAED) patterns were collected with a JEM 2100 microscope (JEOL, Japan) operated at accelerating voltage of 200 kV. Particles were dispersed in ethanol before the experiment and a droplet of an aqueous sol placed on a carbon coated Ni grid (Ted Pella Inc., USA) and allowed to dry at room temperature. Scanning electron microscopy (SEM), EDS and elemental mapping were made utilizing a Hitachi TM 3000 instrument operated at the acceleration voltage of 15 kV, equipped with a Bruker Quantax 70 analyzer.

X-ray photoelectron spectra were acquired with a SPECS instrument (SPECS GmbH) equipped with a PHOIBOS 150 MCD-9 analyzer operated at the pass energy of 20 eV for survey spectra and 10 eV for high-resolution spectra. Monochromatic Al Kα irradiation (1486.7 eV) of the X-ray tube was used for excitation. The pressure in an analytical chamber

was in the range of 10-9 mbar. Samples were placed on sticky carbon tape; hydrosol droplets were dried on highly oriented pyrolytic graphite (HOPG). The atomic concentrations were obtained from the survey spectra. The high-resolution spectra were fitted with Gaussian-Lorentzian peak profiles after subtraction of the Shirley-type background. Spin-orbit splitting and an intensity ratio for S $2p_{3/2,1/2}$ doublet were assumed of 1.19 eV and 2:1, respectively. The Fe 2p spectra were fitted with two sets of multiplet lines (four narrow peaks and a wider satellite)[53] for Fe^{3+} cations bonded to hydroxide anions and Fe^{3+}-S species; possible contributions of Fe^{2+} were taken into consideration too. CasaXPS software was applied for data processing. Electron energy loss spectra in the reflection mode (REELS) were collected using a STAIB electron gun incorporated in the SPECS instrument, with the width at half maximum (FWHM) of elastically reflected beam of 0.7 eV.

^{57}Fe Mössbauer spectra were measured in a transmission mode employing an MC-1104Em spectrometer (Cordon, Russia) with a ^{57}Co(Rh) source that was kept at room temperature, while the absorber (powdered valleriites about 3 mg/cm^2 of Fe in thickness) were either at 20 ºC or cooled down to liquid helium temperature (4.2 K). Isomer shifts (IS) are given relative to α-iron at room temperature. Probabilities P of quadrupole splitting P(QS) and magnetic hyperfine fields P(H) were first determined from the experimental spectra and were used to generate a model spectrum and then to fit the results by varying the complete set of parameters.[54]

Magnetization of valleriite samples was measured using a superconducting quantum interference device (SQUID) magnetometer,[55] typically with a magnetic field of 500 Oe in field cooled, FC, and zero field cooled, ZFC, regimes in the temperature range from 4.2 K to 290 K. The magnetic moment was also determined as a function of the magnetic field varied from 0 to 800 Oe.

Raman spectra were collected from dry vallerrites in the backscattering geometry with a Horiba Jobin-Yvon T64000 spectrometer (Horiba, Japan) equipped with a liquid nitrogen cooled charge-coupled device detection system in subtractive dispersion mode. CW DPSS laser (Spectra-Physics Excelsior-532-300-CDRH) with λ = 532 nm and power of 1 mW on a sample was used as an excitation light source.

Dynamic light scattering (DLS) and zeta potential measurements were performed using Zetasizer Nano ZS spectrometer (Malvern Instruments, UK) at scattering angle 173° in a polycarbonate cell with Pd electrodes at 25 ºC. UV−vis-NIR absorption spectra of hydrosols were collected in the range 200 - 1400 nm in a thermostatic quartz cell with the optical path of 1 cm using a Shimadzu UV 3600 instrument.

3. Results

3.1. Morphology, phase and chemical composition

Figure 2 shows typical X-ray diffraction patterns and TEM micrographs of the hydrothermal products. XRD, as well as electron diffraction (not shown in Figures), revealed reflections of valleriite as the only or predominant crystalline phase, which are in full agreement with the literature,[20] for the reaction mixtures contained atomic proportions of Fe/Cu of 1-2, Fe/Mg of about 1±0.25 and a big excess of sulfide. Extra peaks at the diffraction patterns are minor, if any, as, for example, the one of brucite $Mg(OH)_2$ near 2 theta of 18º (sample a). Valleriite forms within 2 h heating and the XRD reflections became narrower as the reaction proceeds.

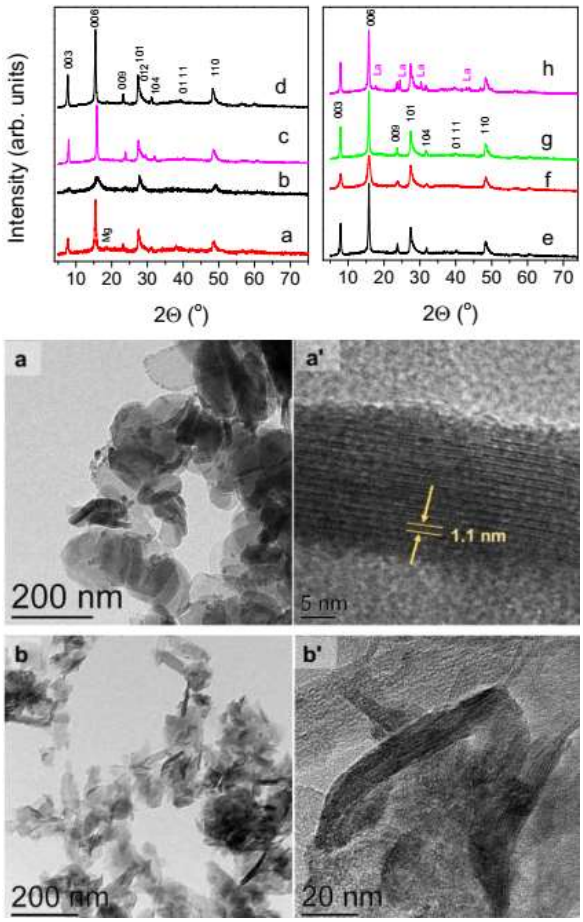

Figure 2. X-ray diffraction patterns and representative TEM images of valleriite samples synthesized (a) without Al, (b) with Al and (c, d) various initial ratios of Fe, Cu, Mg precursors. Right XRD panel illustrates the effect of additional metals: (e, f) Cr, (g) Co and (h) La; reflections of Mg and La hydroxides are marked as Mg (a) and La (h). Please see Table 1 for details regarding the sample preparation and designations.

TEM micrographs show plain particles of 50-200 nm in the lateral size together with elongated ones with the width of 10-25 nm. The latters are not nanorods but the same particles exposing the edge; this is obvious from the TEM images taken from tilted specimens (Figure S2). TEM on the particle edge (a', b') revealed the interatomic distances of about 1.1 nm typical for valleriite structure.[20-25,39] The particles are usually 10-20 layers thick, and both the lateral dimension and thickness increase with the reaction time. In the samples showing insignificant X-ray reflections of brucite, a number of tiny nanoparticles observed around the larger ones appear to be magnesium hydroxide. The size and shape of the particles also depend on composition of the reaction media. Particularly, the particles became smaller and less regular as Al was introduced, but no new (crystalline) phases emerged for the reaction ratio Al/Mg less than 1. XRD reflections widened (compare the samples *a* and *b*) and showed a reduction of some interplanar distances, e.g. [006], due to disordering the hydroxide structure caused by smaller Al^{3+} cations. Additional phases were not detected by XRD upon substitution of Fe with transition 3d metals (the contents of Co and Cr up to 30% of Fe were tested). A main share of rare-earth metals (La, Gd), as well as Si, formed their own hydroxide phases (see Figure 2, h as an example) rather than entered valleriite.

Table 2. Concentrations of elements (C and O are disregarded) in the products determined using EDS and XPS; see Table 1 for description of the samples

Sample	Concentrations (at.%)						
	Fe	Cu	S	Mg	Al	Na	Co
a	23.6	12.5	33.9	30.0	-		
XPS	12.7	8.3	37.8	41.2	-	-	
b	14.6	9.4	26.4	27.2	20.4	-	-
XPS	10.2	6.2	34.1	31.4	18.1	-	-
g	16.2	19.3	34.5	18.8	8.8	0.7	1.7
XPS	9.3	15.2	36.0	21.4	15.0	2.2	0.9

The chemical composition of several valleriite samples determined using EDS analysis are given in Table 2. The compositions generally fall within the range reported in the literature.[27,30] They can substantially differ from the initial proportions of precursors used in the synthesis as excessive amounts of S, Al, partially Fe, Mg are rejected together with Na. Nevertheless, dosing the reagents allows tuning the product composition; in particular, valleriites have deficit of Fe regarding $CuFeS_2$ for the initial proportion Fe/Cu ≈1 (b, g), and excess of Fe for the proportion Fe/Cu =2 (a), although the magnitude of non-stoichiometry is not so big. The samples may contain small quantities of Na and sulfate uptaken by the nanoscale solids with high surface areas or/and the remnants of aqueous media. Table 2 shows also surface concentrations derived from XPS, which principally confirm the above. Elemental maps (Figures S3, S4, Supporting Information) indicate quite uniform spatial distribution of elements, including dopants.

3.2 XPS and REELS

XPS analysis found the concentrations in reasonable agreement with the EDS data, but the deficit of iron and excess of sulfur are larger (Table 2, Figure 3), probably, due to oxidation of the probed outer layers exposed to the environment. The spectra of copper are essentially the same for all the samples, with the major Cu $2p_{3/2}$ peak (more than 80% of intensity) at the binding energy (BE) of 932.5 eV ± 0.1 eV and Cu L_3MM Auger peak at 917.0 eV. Shake-up satellites at 944-948 eV are negligible so the 3d states are (almost) completely occupied. These specify Cu^+ cations bonded to sulfur.[38,56-59] The Cu $2p_{3/2}$ maxima are slightly broadened at higher BEs that is typical for many copper sulfides due to minor Cu^{2+}/Cu^+-O species and/or shake-off satellites.[56,57]

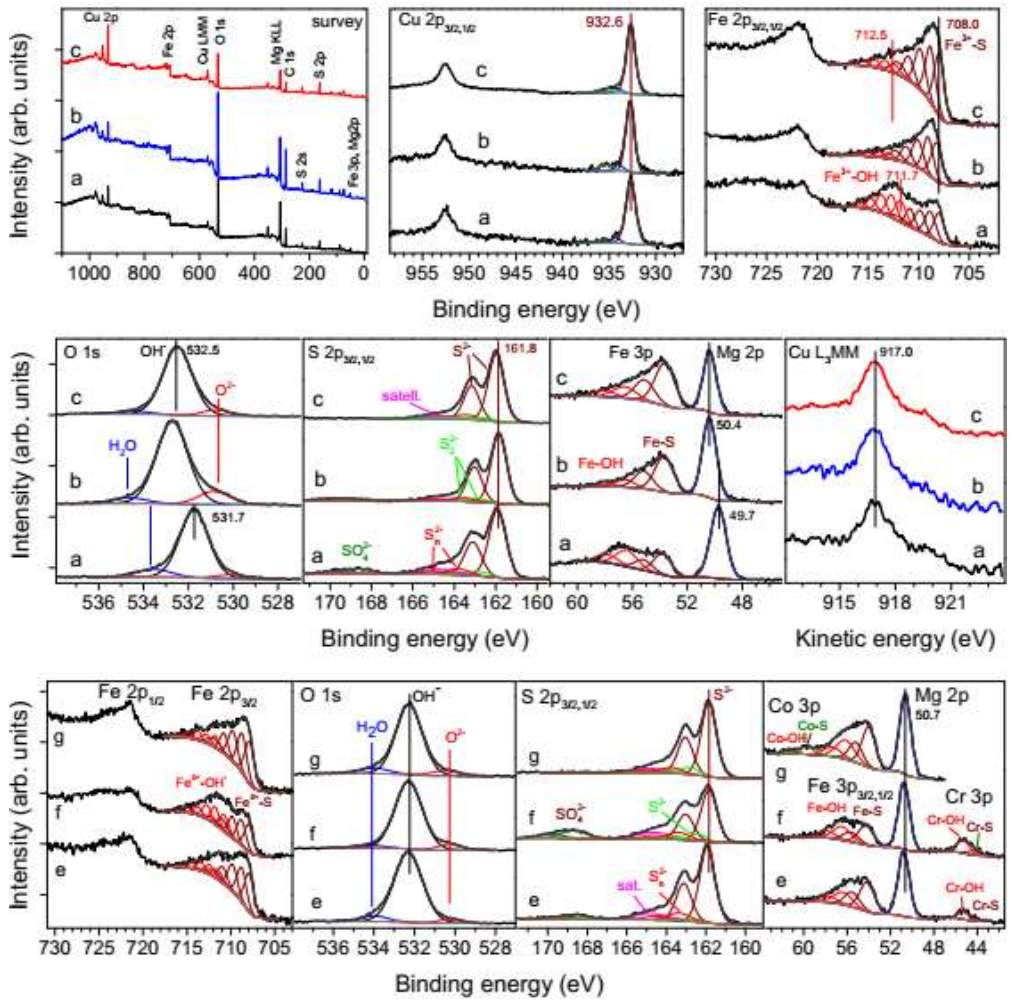

Figure 3. X-ray photoelectron spectra of valleriites synthesized with different proportions of Fe and Cu precursors without Al (a) and with Al (b, c, e, f, g) and also doped with (e), (f) Cr and (g) Co. The designations a, b, etc. correspond to the samples listed in Table 1 and 2. The spectra of sample (d) (Table 1), which are similar to those of sample (c), are omitted.

The Fe $2p_{3/2}$ bands can be fitted using two five-line multiplet sets including wider high-energy satellites[53] with the first peaks at 708 eV and 711-712 eV attributable to Fe^{3+} centers bonded with sulfide and hydroxide anions, respectively.[53,59,60] The position of the Fe-S lines is almost the same in all valleriites while the BEs of Fe^{3+}-OH lines can vary by more than 1 eV concurrently with those of Mg 2p and O 1s as described below. This means, among other things, that these Fe atoms occur in the hydroxide layer of valleriite but not in a separate phase. The fitting with numerous peaks is not unambiguous, and minor Fe^{2+}-S and Fe^{2+}-O species may be missed. The Fe 3p spectra, which don't have complicated multiplet structure and characterize somewhat thicker probing depths due to higher kinetic energies (lower BEs) of photoelectrons, are composed of wide maxima and also are inconclusive in terms of possible minor components. Both the Fe 2p and 3p spectra show that from 55% to 90% of iron atoms are located in the sulfide sheets as predominant Fe^{3+} species, and the rest are in brucite-like layers. The relative concentration of the S-bonded Fe increases with addition of Al, a decrease of the initial precursor proportion Fe/Cu, and, in a lesser extent, with prolonging the reaction time.

The main S 2p doublet with the BE of S $2p_{3/2}$ peak at 161.7±0.1 eV amounts up to 80% of the total intensity, which decreases in case of a large share of Fe-O species whereas the small components at about 162.5 eV and 163.5 eV from di- and polysulfide species, respectively,[58-60] grow. The S 2p spectra are better fitted using an additional broad maximum centered near 164.5 eV that appears to arise from a satellite related to electron transfer to vacant Fe 3d states.[56-60] Up to 10% of sulfur presented as sulfate anions adsorbed from the solution. Therefore, the sulfide part of valleriite is often depleted in metals, mainly Fe that could transfer to hydroxide sheets and then to the environment from the near-surface layers, leaving S-S bonding. The deficit of Fe in the sulfide sheets can be diminished by using, first of all, an Al modifier in the synthesis.

While the photoelectron lines of Cu, S and Fe-S species stay within a narrow range of ±0.1 eV, the BEs of Mg 2p and O 1s peaks, as well as of Fe^{3+}-OH signals, increase up to ~1 eV as Al was added. The effect should be assigned to a shift of the Fermi level toward a higher energy in the brucite-like structure (see Figure S5) rather than changes of the chemical state of the elements. The O 1s spectra show, along with the major signal of OH^- groups shifted from 531.5 eV to ~532.5 eV, an increased contribution from O^{2-} species at a binding energy of ~530.5 eV. The high-energy shifts fade with extending the synthesis time, probably because the particles grow and the impact of surfaces decreases, but the influence of Al on the distribution of iron between hydroxide and sulfide maintains. These findings suggest a negative, or less positive, charging of the Al-bearing hydroxide layers due to a transformation of OH^- into O^{2-} anions releasing protons, and distortions of the hydroxide structure via displacement of Mg^{2+} and Fe^{3+} species by smaller Al^{3+} cations.

XPS of Cr- and Co-doped samples found (Figure 3, lower panels) that about 80% of Cr enters Al-bearing hydroxide layers (Cr 3p spectra of the samples e, f in the lower wright-hand panel); this results in increasing proportion of Fe^{3+}-OH species, probably due to decreasing content of Al. Two thirds of cobalt go into sulfide sheets (spectra *g*), and 80% of Fe remains S-bonded, at least for the moderate concentrations of the dopants used (Table 1). Rare earth metals and Si form separated hydroxide phases, and XPS can't distinguish minor quantities of the elements in the doped valleriites.

Figure 4 shows electron energy loss spectra measured in the reflection mode (REELS) aligned to zero energy loss and normalized by the intensity of the reflected elastic peak. The spectra were acquired using the primary electron beam energy from 3 000 eV to 300 eV, and so the probing depths from about 5 nm to 1 nm. The energy band gap (E_g) can be determined from the REELS spectra by approximating the slope of maxima by a straight line and assigning E_g to values at the intersection with the energy axis.[61] The two linear plots may correspond to two band gap energies of 0.25 ± 0.2 eV and 4.2± 0.5 eV which can be tentatively attributed either to sulfide and hydroxide parts, or, more likely, to the narrow gap between the valence band (VB) and the "intermediate" empty Fe 3d band, and the wide fundamental gap, respectively, by analogy with chalcopyrite.[56,58-60] The first E_g value satisfactorily complies with the optical band gap (see Figure 8). The REELS spectra exhibit also a distinct maximum with the energy losses of ~2.5 eV and ~2.1 eV for the samples synthesized with (a) and without Al (b), again in agreement with the optical UV-vis-NIR absorption.

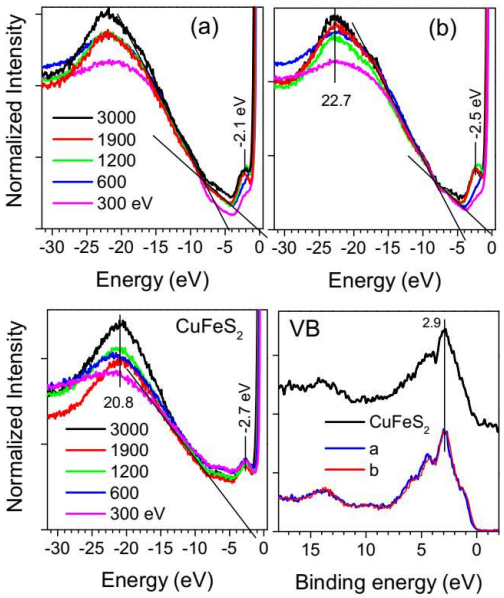

Figure 4. Reflection electron energy loss spectra and XPS spectra of the valence band (VB) of vallerite samples (a) without and (b) with Al (Table 1), in comparison with the spectra of bulk chalcopyrite $CuFeS_2$. REELS was measured using varying energy of the incident electron beam marked in the plots.

It is interesting to compare REELS and photoelectron spectra of the valence band of valleriites with those of chalcopyrite $CuFeS_2$ (lower panels). The plasmon maximum of chalcopyrite has a lower energy of 20.8 eV vs. 22.7 eV in valleriites due to diverse dielectric properties, which are not considered here. The narrow band gap of chalcopyrite (about 0.5 eV)[56,57] cannot be reliably determined from the REELS. The total density-of-states (DOS) in the VB region are rather similar for both compounds as the main contribution is due to Cu 3d states peaked at 2.9 eV below the band edge, and they have small differences near the Fermi level and at BEs of 4-5 eV where the density of Fe 3d states is significant. The position of the REELS feature at 2.7 eV is close to the DOS maximum for chalcopyrite but the one at 2.1-2.5 eV notably differs from the VB peak for valleriites; it also should be kept in mind that REELS is insensitive to the Fermi energy position and electrostatic charging,[61] in contrast to photoelectron spectra. The origin of the features will be further discussed below in relation with UV-vis spectra of valleriite colloids.

3.3. Mössbauer spectroscopy and magnetic measurements

^{57}Fe Mössbauer spectra (Figure 5, Table S1) of the valleriites without impurity phases shed new light onto state of iron in comparison with the previous work on natural mineral assemblages and synthetic samples.[26,35-37,39] The asymmetric central signals observed at room-temperature can be fitted using 2 or 3 doublets with isomeric shifts (IS) and quadrupole splitting (QS) of IS = 0.34±0.03 mm/s and QS = 0.55±0.06 mm/s, and IS = 0.4±0.05 mm/s and QS = 1.1±0.1 mm/s (Figure 5, a-c), which should be assigned, from comparison their intensities with the XPS spectra (Figure 3), to paramagnetic Fe^{3+} centers in tetrahedral coordination with S and octahedral coordination with OH^-, respectively. The spectra from the samples (a, b) prepared with excessive Fe precursor (i. e., Fe/Cu=2) are better fitted by using additional weak signals with a small or zero QS, which may be due to minor low-spin Fe^{2+} centers. The spectra of the

samples prepared with Cr, Co, La dopants can be fitted using an additional doublet with QS > 1.2 mm/s possibly from Fe centers irregularly surrounded by different cations.

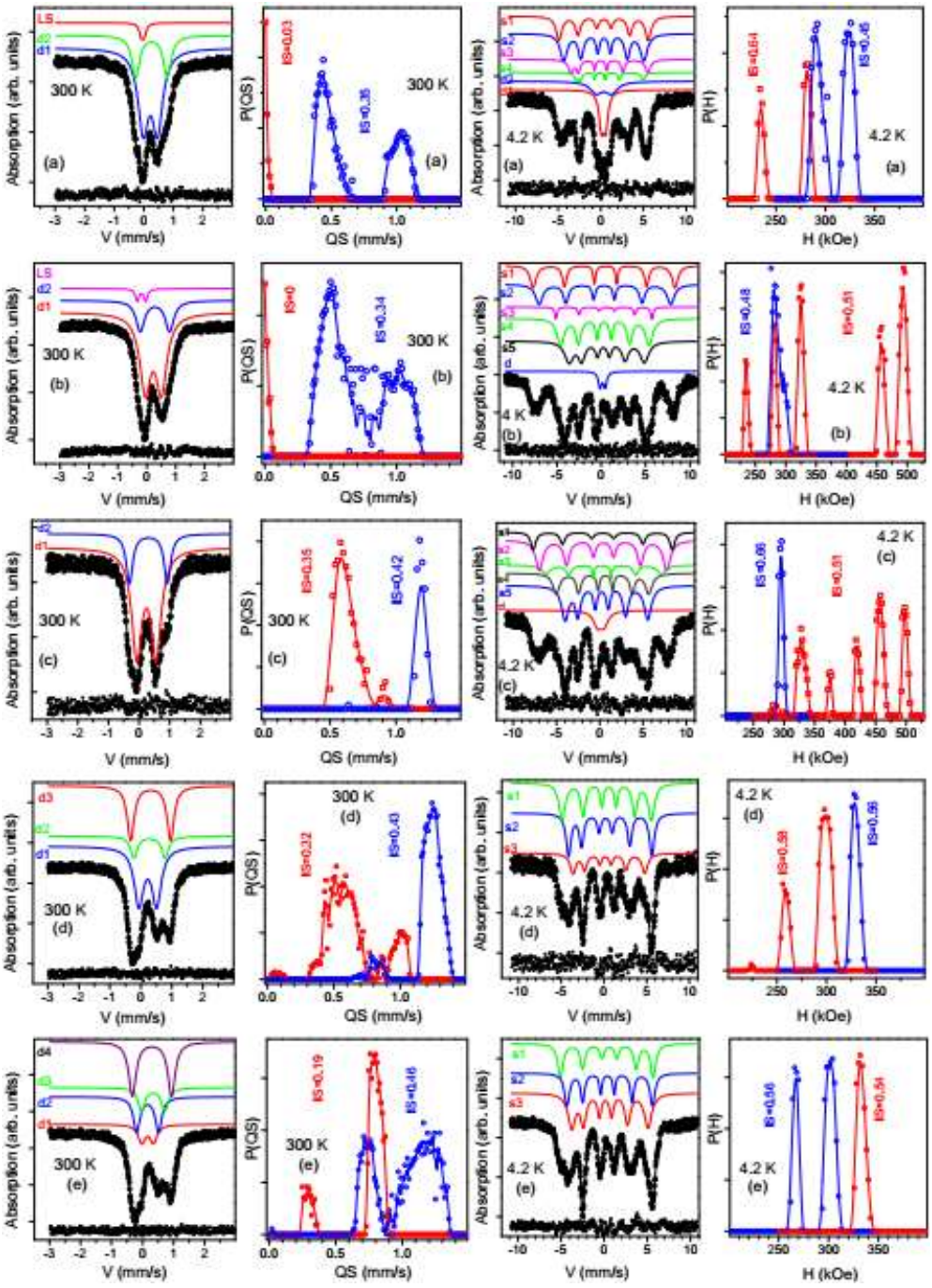

Figure 5. Mössbauer spectra of synthetic valleriites containing (a) no Al, (b), (c) with Al, (d) Cr, (e) La measured at room temperature (left panels) and 4.2 K, and the probabilities of quadrupolesplitting P(QS) and hyperfine field P(H). Colored lines are the results and points below the spectra are the errors of fitting; the best fit parameters are given in Table S1. The designations (a), (b), (c), (d), (e) correspond to the samples a, b, c, e, h listed in Table 1, respectively.

The spectra collected at 4.2 K consist of a series of Zeeman six-line components and minor doublets. The intensities of the sextets with smaller QS correlate with those of doublets associated with Fe^{3+}-S centers at 300 K, whereas the ones with QS > 1 mm/s are likely due to Fe^{3+} in hydroxide sheets, in agreement with the room-temperature Mössbauer and photoelectron spectra. The emergence of sextets means transitions to ordered magnetic states involving a variety of Fe positions in the 2D layers. Interestingly, for Al-containing valleriites (samples b, c), almost half of Fe centers in the sulfide sheets exhibit the hyperfine magnetic fields H as high as ~500 kOe, while the spectra (d),(e) of the samples with additional magnetic cations (Cr, Ln) show no high field magnitude sextets.

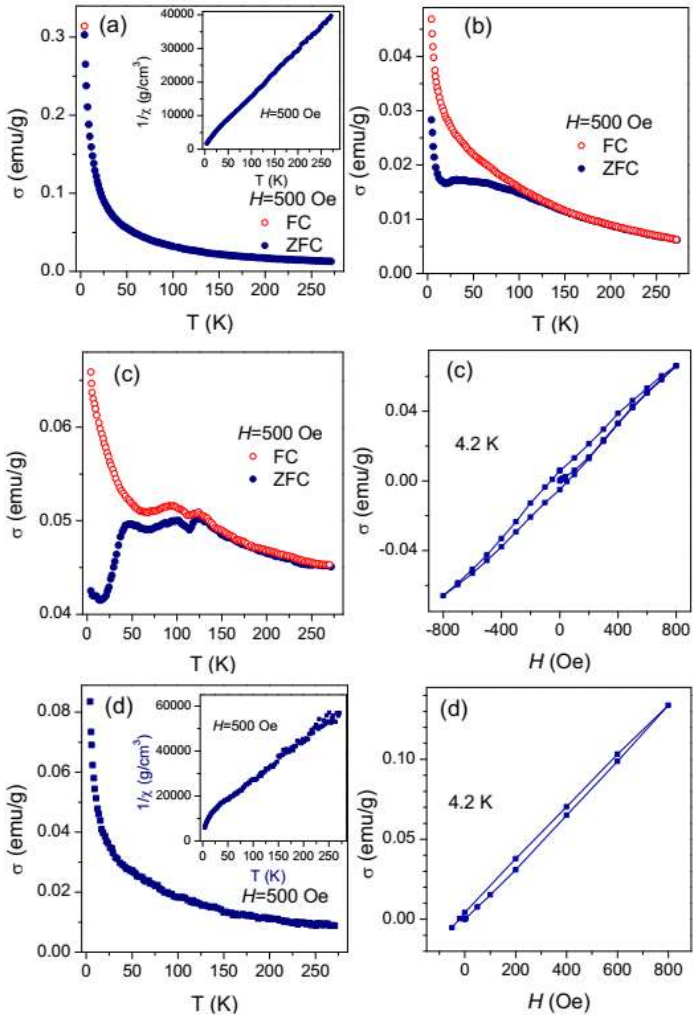

Figure 6. Temperature (FC and ZFC) and field dependences (hysteresis loops at 4.2 K) of magnetization of valleriite samples (a) without Al, (b), (c) containing Al; sample (d) is Cr doped. Insertions in (a) and (d) show reciprocal susceptibility 1/χ vs temperature plots. The samples (a), (b), (c) and (d) correspond to those marked as (a), (b), (c) and (e) in Table 1 presenting the preparation details.

Typical temperature dependences of magnetization of valleriite samples and magnetic hysteresis loops at 4.2 K are presented in Figure 6. Almost coinciding, pure paramagnetic FC and ZFC curves were observed for the samples with no Al and larger content of Fe in hydroxide layers. The more complicated behavior of valleriites, which contain Al and exhibit Zeeman

sextets with internal magnetic fields of 400-500 kOe in the Mössbauer spectra, may be interpreted in terms of paramagnetic, superparamagnetic and also minor ferromagnetic contributions[62-64] below ~120 K. Bulk antiferromagnetism that is characteristic of Cu-Fe sulfides ($CuFeS_2$, Cu_5FeS_4)[40,65] is not observed, possibly because of the strong paramagnetic signal, but local antiferromagnetic interactions cannot be ruled out. Valleriites doped with Cr (Figure 6, *d*) are mainly paramagnetic but show small ferromagnetic features (a drop of the reciprocal magnetic susceptibility $1/\chi$ and a hysteresis loop) below 20 K. Since high hyperfine fields were not found in the ^{57}Fe Mössbauer spectra (Figure 5, *d*), this ferromagnetism may be due to Cr centers. Thus, Mössbauer and magnetic measurements reveal peculiar spin effects related with distribution of iron centers in the 2D layers and possible size effects.

3.4. Raman spectroscopy

Raman spectroscopy is an important tool for characterization of 2D materials that it sensitive to their atomic and electronic structures, number of layers and so forth.[66] Figure 7 compares the Raman spectra of synthetic vallerriites having excess of Fe without (*a*) and with Al (*b*) and so high and low relatively contents of Fe in hydroxide layers, with total deficit of Fe (*c*) and Co-doped valleriite (sample d; please consult Table 1 for details), and a natural valleriite[67] and chalcopyrite[68-71] for comparison. The spectra of valleriites are composed of three main broad maxima at about ~255, 290 and 330 cm^{-1}, and weaker ones at 80 and 140 cm^{-1}. The maxima are better resolved for bulk minerals and synthetic Al-free valleriite with more prefect crystalline structure. The positions of maxima only slightly differ for the synthetic nanoflakes and the bulk mineral but relative intensities change considerably. It would be instructive to compare the Raman spectra of valleriites with that of chalcopyrite, $CuFeS_2$,[69-71] whose main peak at 292 cm^{-1} and smaller ones at 315-380 cm^{-1} are believed to arise from the A_1 mode and B_2/E modes, respectively, of the Fe-S bond vibrations, and the weaker feature near ~270 cm^{-1} is likely due to the Cu-S bond (B_2 mode).

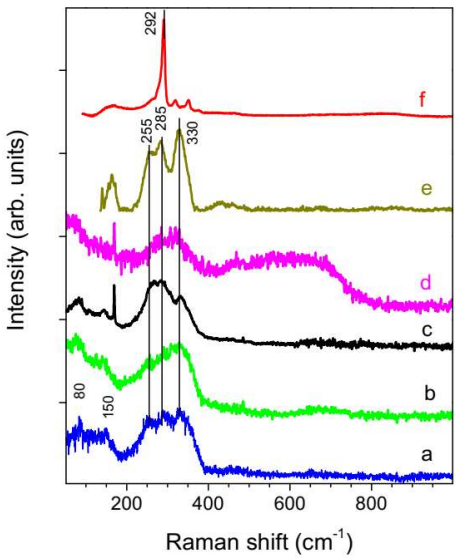

Figure 7. Raman spectra of valleriites synthesized using (a) no Al and Fe/Cu =2 precursors, (b) Fe 2, Cu 1, Al 2, (c) Fe=Cu=2, Al 0.5, (d) Al and Co-doped valleriite, (e) natural valleriite[67] and (f) chalcopyrite $CuFeS_2$.[68] Narrow peaks at ~170 cm^{-1} in the plots (c) and (d) are artefacts due laser harmonics. The spectra marked as (a), (b), (c) and (d) correspond to the synthetic samples (a), (b), (d) and (g) listed in Table 1, respectively.

In the 2D sulfide layers of valleriite, the central peak appears to originate mainly from the Fe-S bond vibrations of the A_g type too, with metal atoms moving in the plane and S atoms shifting normally to the sheet. The maxima at ~255 cm^{-1} and 330 cm^{-1} in the spectra of valleriite may be tentatively assigned to vibrations of Cu-S and Fe-S bonds, respectively. This corroborates with enhanced maxima at ~255 cm^{-1} for the samples (a) and (c), which have the sulfide layers depleted in Fe and enriched in Cu. So, Raman spectroscopy can provide information both on composition and structure of the sulfide sheets; unfortunately, weak scattering from hydroxide part was practically undetectable.

3.5. Colloidal solutions

Both hydrosols spontaneously formed during washing of valleriite and those produced by ultrasonic treatment of the residue in 2 mM sodium dodecyl sulfate (SDS) solutions were studied using DLS, zeta-potential measurement, XPS and TEM. Clear differences between the colloidal particles synthesized without and with Al, that is, with high and low content of Fe in hydroxide layers, were observable in both cases but more pronounced for the surfactant-free colloids. The hydrodynamic diameters D_h (Figure 8, panel (*a*)) varied from about 70 nm for Al-bearing particles to ~150 nm for Al-free ones, in general agreement with TEM data (Figure 2). The former particles showed more negative zeta-potential (about -40 mV vs -30- -35 mV) (Figure 8, (b)). For SDS-capped particles, D_h magnitudes were almost the same but their zeta-potentials were in the range from -20 mV to -35 mV with a smaller distinction between Al-containing and Al-free valleriites (Figure 8, (d), (e)). The negative zeta-potentials for colloids both with and without SDS are almost independent of pH in the range of 3 to 11 (dissolution yielding H_2S and covellite CuS started at pH < 3). This is surprising because brucite having the isoelectric point at pH ≥ 11[72] should be charged positively in the pH region utilized here, and it seems unlikely that the outermost hydrophilic surface of valleriite is formed by sulfide sheets. The problem cannot be ultimately resolved using TEM images and XPS spectra of the colloidal particles, which are generally similar to those of the relevant precipitates (Figure 2, a' and Figure 3).

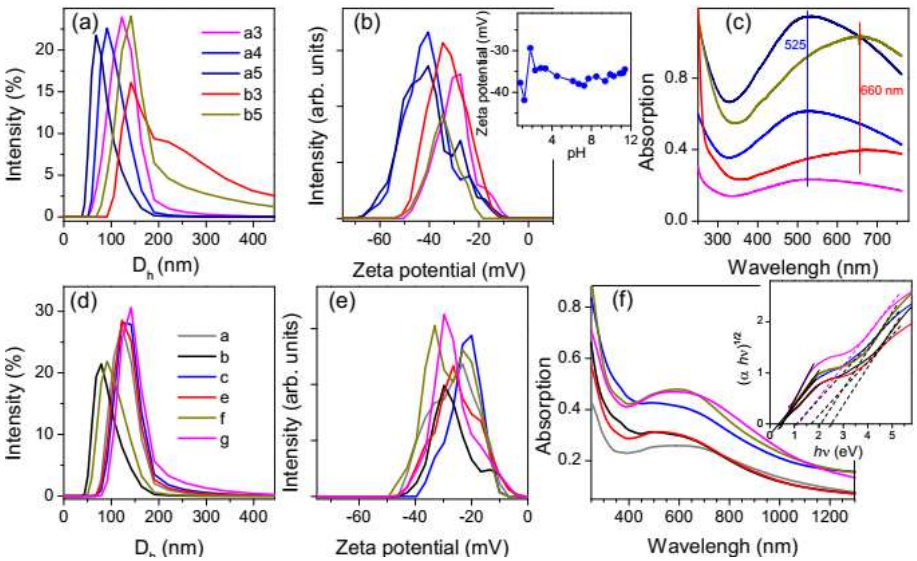

Figure 8. Distributions of (a), (d) hydrodynamic diameter D_h, (b), (e) zeta potentials and (c), (f) UV-vis-NIR absorption spectra of valleriite hydrosols spontaneously formed during the

water washing (upper panels (a)-(c)), and prepared using sonification of corresponding final residues in aqueous 2 mM SDS solution (lower panels (d)-(f)). In upper panels, samples were synthesized (32 h) using the initial precursor ratios: *a3-a5* - Al 0.5, Fe 2, Cu 2, Mg 2, S 14; *b3,b5* - Al 0, Fe 2, Cu 2, Mg 2, S 14, with indexes 3,4,5 standing for a number of washing cycle in which this sol was formed. In lower panels, hydrosol sample *a* contained no Al, *b,c* – Al-containing, *e,f* – Cr-doped, *g* – Co-doped (the designations are the same as in Table 1). pH 10.5±0.2, 25 ºC.

UV-vis spectra (Figure 8, panels (c) and (f)) show absorption maxima centered at ~520 nm (2.5 eV) for the particles containing Al and 600-700 nm (~2 eV) if no Al was added; Cr- and Co-doped particles show red-shifted absorption despite the presence of Al. Analogous optical response with the absorption band at ~500 nm has been found for nanocrystals of chalcopyrite $CuFeS_2$ and assigned to localized surface plasmon resonance (LSPR)[73,74] albeit low free carrier densities in the semiconducting chalcogenides. Alternatively, a quasi-static dielectric resonance associated with an intermediate band of empty Fe d-states has been suggested to cause the optical absorption in the visible region.[75-77] The spectra shift to larger wavelengths with decreasing content of Fe,[77] and the NIR absorption for copper chalcogenides with no or low Fe concentration has been attributed to LSPR from electron holes in the VB related with Cu vacancies,[77-79] although this is doubtful too[58] because of the lack of correlation between the peak position and intensity expected for LSPR. The energies of the optical absorption of valleriite colloids coincide with the electron energy loss bands at 2.0-2.5 eV in REELS (Figure 5), and it is unlikely that these features are due to LSPR.

Tauc plots,[80] which allow determining the band gap width, are presented in Figure 8, f as the $(\alpha h\nu)^{1/2}$ vs $h\nu$ graphs for indirect band gap. The x-axis intersection points of the linear fit in the vis-NIR region give the band gap values of 0.4±0.1 eV for all the samples that is close to the gap width of chalcopyrite and correlates with the results of REELS. The high energy regions appear uninformative (the gap values varied from 1 to 3 eV) because of overlapping the absorption maxima.

4. Discussion

The above findings on the synthesis, main properties and potential applications of valleriite-based materials following from the research are summarized in Figure 9. The flake-like nanoparticles composed of altering quasi-atomic Cu-Fe-S sulfide and Mg hydroxide sheets are manufactured in the environment-friendly hydrothermal process using common reagents. Such a chalcogenide-hydroxide incommensurate structures looks unusual and complex but there exist a number of natural[20-34] and synthetic[43-51] layered materials, suggesting that those are quite stable and spontaneously assemble via a mechanism that needs to be understood. The composition and then morphology and properties of the materials can be engineered by varying the nature and concentrations of precursors, modifiers, dopants far beyond those used in this case study. In general, these 2D materials are still scarcely studied and their potential is highly underestimated.

The current research demonstrates, in particular, that the distribution and state of iron in the hydroxide and sulfide parts affect many characteristics of valleriites, which can be modified by changing the initial proportion of Fe and Cu precursors, doping with transition metals and, interestingly, modifying the hydroxide layers, especially with smaller aluminum cations. It has

been accepted in the literature that the hydroxide component bears a positive electrical charge due to Al^{3+} and/or Fe^{3+} replacing Mg^{2+} cations. However, XPS and zeta potential measurements are indicative of its negative charge and a likely positive charge of sulfide sheets. We hypothesize that the excessive charge of trivalent cations is neutralized by O^{2-} species detected in XPS and additional OH^- anions in the hydroxide sheets, distorting the brucite-like structure. Monovalent modifiers akin to Li^+ are expected to have an opposite effect; such research is now underway in our laboratory.

Electronic, magnetic and optical properties of the composites are apparently determined by the 2D transition metal sulfide component that exhibits the narrow forbidden band on the order of 0.4 eV close to that of chalcopyrite. This concurs with DFT+U simulation (to be published elsewhere) found that the gap between the VB and unoccupied Fe 3d band is ~0.9 eV for an ideal atomic $CuFeS_2$ sheet with ordered electron spins of Fe atoms and it decreases due to disordering. The sulfide properties are expected to depend also on the metal (primarily Fe) vacancies, S-S bonding, transition metal doping, and the electron density induced by hydroxide counterparts. The sulfide layers are in a kind of electron equilibrium with the brucite-like ones, and the Fermi level E_F effectively pinned in the narrow-gap sulfide varies within the wide-gap Mg-based hydroxide due to changing the concentrations of foreign elements, particularly Fe and Al (Figure S5). Despite comparably small shifts of the E_F in the sulfide sheets, the corresponding electron density changes should strongly affect their properties.

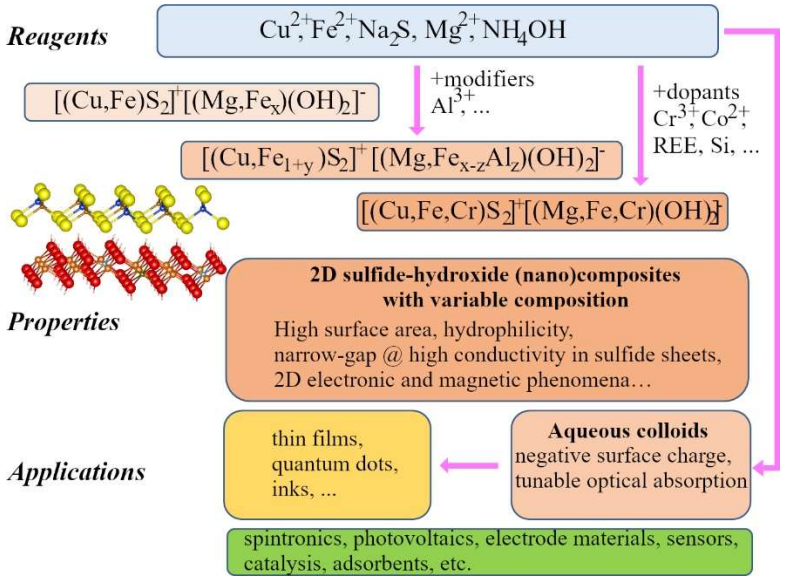

Figure 9. Scheme illustrating the main factors influencing the production, composition and properties of valleriites as explored in this work, and their potential applications.

The nanoscale products easily form aqueous colloids either spontaneously without additional stabilizers (mechanisms behind this effect are not quite clear yet), or via peptization of the precipitates with a surfactant. Both sorts of colloids show unexpected negative pH-independent zeta-potentials, and optical absorption in visible and NIR spectral region, with the energies of the optical resonance of 2-2.5 eV agree with those observed in REELS. The origin of the maxima and their shift to lower energies with increasing content of iron in hydroxide layers may be rationalized in terms of quasi-static dielectric resonance.[75-77] To the best of our knowledge, these phenomena have been not studied for 2D composites, and their nature needs

to be clarified. The tunable optical response of nanoscale valleriite is prospective for plasmonics, energy conversion, sensors and theranostics.

Consequently, the numerous characteristics of valleriite-type 2D composites can be tailored through the total chemical composition, distribution of Fe in the sulfide and hydroxide layers, insertion of foreign cations, size and morphology of the (nano)particles and other factors. In comparison with graphene, transition metal dichalcogenides, MXens, double layered hydroxides and so forth, valleriites and related materials appear to have more diversified features suitable for potential applications in electronics, spintronics, energy storage, and so on. It is worth recalling, for example, that similar composite of metal (Li and others) hydroxide and iron selenide monolayers are superconductors.[43-51] The large surface area, layered structure, and specific surface properties are essential for applications of the nanoscale valleriites as adsorbents, catalysts, sensors, electrode materials, etc. The feasible peptization of the materials paves the way for their utilization as quantum dots and inks or manufacturing thin films on various supports. The last but not the least is that the metal sulfide sheets embedded between hydroxide layers are more stable towards oxidation. The valleriite-based composites emerge, therefore, as a novel platform for 2D materials with a very rich spectrum of prospective and, maybe, unique properties. At the same time, a lot of questions regarding the formation mechanisms, structure, physical and chemical properties and their tailoring still need to be answered.

5. Conclusions

We propose a simple method of green hydrothermal synthesis of valleriite particles (50-200 nm in the lateral size and 10-20 nm thick) composed of altering 2D sheets of Cu-Fe sulfide and Mg-based hydroxide. The sulfide sheets close to $CuFeS_2$ composition contain Cu^+ and Fe^{3+} cations and monosulfide anions along with minor S-S species, formed in conjunction with cationic (most often Fe) vacancies. XPS and Mössbauer spectroscopy found that ferric iron is distributed between sulfide (55-90%) and hydroxide layers; the content of Fe-OH can be reduced, in particular, by addition of Al. Valleriite was modified with transition 3d metals (Cr, Co) entering both sulfide and hydroxide layers, whereas only insignificant quantities of rare-earth elements and Si were incorporated into hydroxide layers. The electronic and magnetic characteristics of the composites are largely determined by the sulfide component that has the forbidden band gap of about 0.4 eV as derived from REELS and optical UV-vis-NIR spectra. Room-temperature Mössbauer spectra comprise of central signals of paramagnetic Fe in the sulfide and hydroxide layers, which transform to a series of Zeeman sextets due to magnetic ordering at 4.2 K, with the sextets with higher, up to 500 kOe, hyperfine magnetic fields originating from the sulfide layers. SQUID measurements revealed pure paramagnetism and more complicated behavior in composites containing considerable and small amount of Fe in hydroxide part, respectively. Raman spectra were found sensitive to structural order and Fe/Cu ratio in the sulfide layers. Colloidal solutions of valleriite, both spontaneously formed during the product washing and prepared by sonification of the precipitates in sodium dodecyl sulfate solutions, have negative zeta potentials almost independent on pH, suggesting a negative charge of hydroxide sheets, in agreement with the shift of relevant photoelectron lines. UV-vis-NIR spectra show absorption maxima between ~500 nm and ~700 nm, whose energies concur with the loss maxima at 2-2.5 eV in REELS, tentatively attributed to the quasi-static dielectric resonance involving “intermediate” empty Fe 3d band. So, the nanoscale sulfide-hydroxide composites unveiled a number of controllable electronic, magnetic, optical,

interfacial properties interesting for many applications, designating valleriites as a novel family of two-dimensional materials.

Supporting Material. Scheme and photos of autoclave set-up (Figure S1), additional TEM images (Figure S2), elemental mapping (Figures S3, S4), scheme illustrating the band structures and changes of binding energies in XPS (Figure S5), Mössbauer parameters (Table S1).

Corresponding Author
Yuri L. Mikhlin - Institute of Chemistry and Chemical Technology, Krasnoyarsk Science Center of the Siberian Branch of the Russian Academy of sciences, Akademgorodok, 50/24, Krasnoyarsk, 660036, Russia; orcid.org/0000-0003-1801-0947; Email: yumikh@icct.ru

ACKNOWLEDGMENT
This research was supported by the Russian Science Foundation for Basic Research, Krasnoyarsk Territory Administration and Krasnoyarsk Territory Science Foundation, project 20-43-242903. Facilities of the Krasnoyarsk Regional Center of Research Equipment of Federal Research Center «Krasnoyarsk Science Center SB RAS» were employed in the work.

REFERENCES
[1] S. K. Tiwari, S. Sahoo, N. Wang, A. Huczko, Graphene research and their outputs: Status and prospect. *J. Sci.: Adv. Mater. Devices* **2020**, *5*, 10-29. https://doi.org/10.1016/j.jsamd.2020.01.006.
[2] A. K. Geim, I. V. Grigorieva, Van der Waals heterostructures. *Nature* **2013**, *499*, 419-425. https://doi.org/10.1038/nature12385.
[3] M. Xu, T. Lian, M. Shi, H. Chen, Graphene-like two-dimensional materials. *Chem. Rev.* **2013**, *113*, 3766–3798. https://doi.org/10.1021/cr300263a.
[4] K. Zhang, Y. Feng, F. Wang, Z. Yang, J. Wang, Two dimensional hexagonal boron nitride (2D-hBN): Synthesis, properties and applications. *J. Mater. Chem. C* **2017**, *5*, 11992−12022. https://doi.org/10.1039/C7TC04300G.
[5] K. S. Burch, D. Mandrus, J. Park, Magnetism in two-dimensional van der Waals materials. *Nature* **2018***, 563*, 47–52. https://doi.org/10.1038/s41586-018-0631-z.
[6] D. L. Cortie, G. L. Causer, K. C. Rule, H. Fritzsche, W. Kreuzpaintner, F. Klose, Two-dimensional magnets: Forgotten history and recent progress towards spintronic applications. *Adv. Funct. Mater*. **2019**, 1901414. https://doi.org/10.1002/adfm.201901414.
[7] Y. Guo, S. Zhou, J. Zhao, Two-dimensional intrinsic ferromagnets with high Curie temperatures: Synthesis, physical properties and device applications. *J. Mater. Chem. C* **2021**, *9*, 6103-6121. https://doi.org/10.1039/D1TC00415H.
[8] Y.-W. Cheng, J.-H. Dai, Y.-M. Zhang, Y. Song, Two-dimensional, ordered, double transition metal carbides (MXenes): A new family of promising catalysts for the hydrogen evolution reaction. *J. Phys. Chem. C* **2018**, *122*, 28113-28122. https://doi.org/10.1021/acs.jpcc.8b08914.
[9] L. Verger, V. Natu, M. Carey, M. W. Barsoum, MXenes: An introduction of their synthesis, select properties, and applications. *Trends Chem*. **2019**, *1*, 656-669. https://doi.org/10.1016/j.trechm.2019.04.006.

[10] H. Kim, H. N. Alshareef, MXetronics: MXene-enabled electronic and photonic devices. *ACS Materials Lett*. **2020**, *2*, 1, 55–70. https://doi.org/10.1021/acsmaterialslett.9b00419.
[11] M.-R. Gao, Y.-F. Xu, J. Jiang, S.-H. Yu, Nanostructured metal chalcogenides: Synthesis, modification, and applications in energy conversion and storage devices. *Chem. Soc. Rev*. **2013**, *42*, 2986-3017, https://doi.org/10.1039/c2cs35310e.
[12] A. A. Tedstone, D. J. Lewis, P. O'Brien, Synthesis, properties, and applications of transition metal-doped layered transition metal dichalcogenides. *Chem. Mater*. **2016**, *28*, 1965-1974. https://doi.org/10.1021/acs.chemmater.6b00430.
[13] D. Monga, S. Sharma, N. P. Shetti, S. Basu, K. R. Reddy, T. M. Aminabhavi, Advances in transition metal dichalcogenide-based two-dimensional nanomaterials. *Mater. Today Chem*. **2021**, *19*, 100399. https://doi.org/10.1016/j.mtchem.2020.100399.
[14] Y. Li, Y. Wang, B. Pattengale, J. Yin, L. An, F. Cheng, Y. Li, J. Huang, P. Xi, High-index faceted $CuFeS_2$ nanosheets with enhanced behavior for boosting hydrogen evolution reaction. *Nanoscale* **2017**, *9*, 9230-9237. https://doi.org/10.1039/C7NR03182C.
[15] Z. Du, S. Yang, S. Li, J. Lou, S. Zhang, S. Wang, B. Li, Y. Gong, L. Song, X. Zou, P. M. Ajayan, Conversion of non-van der Waals solids to 2D transition-metal chalcogenides. *Nature* **2020,** *577*, 492-496. https://doi.org/10.1038/s41586-019-1904-x.
[16] T. Gao, Q. Zhang, L. Li, X. Zhou, L. Li, H. Li, T. Zhai, 2D ternary chalcogenides. *Adv. Optical Mater.* **2018**, *6*, 1800058. https://doi.org/10.1002/adom.201800058.
[17] Z. He, W. Que, Molybdenum disulfide nanomaterials: Structures, properties, synthesis and recent progress on hydrogen evolution reaction. *Appl. Mater. Today* **2016**, *3*, 23-56. https://doi.org/10.1016/j.apmt.2016.02.001.
[18] R. Kumar, N. Goel, M. Hojamberdiev, M. Kumar, Transition metal dichalcogenides-based flexible gas sensors. *Sens. Actuator. A Phys*. **2020**, *303*, 111875. https://doi.org/10.1016/j.sna.2020.111875.
[19] S. Stolyarova, A. Kotsun, Y. Shubin, V. Koroteev, P. Plyusnin, Y. Mikhlin, M. Mel'gunov, A. Okotrub, L. Bulusheva, Synthesis of porous nanostructured MoS_2 materials in thermal shock conditions and their performance in lithium-ion batteries. *ACS Appl. Energy Mater*. **2020**, *3*, 10802–10813. https://doi.org/10.1021/acsaem.0c01837.
[20] H. T. Evans, Jr., R. Allman, The crystal structure and crystal chemistry of valleriite. *Z. fur Kristallogr*. **1968**, *127*, 73-93. https://doi.org/10.1524/zkri.1968.127.1-4.73.
[21] A. D. Genkin, L. N. Val'sov, O Valleriite i Machinovite i Usloviyakh ikh Nakhozhdeniya v Rudakh (On Valleriite and Makhinovite and Conditions of their Presence in Ores). *Geol. Rud. Mestorozhd*. **1967**, *9* (2), 94-106 (in Russian).
[22] L. J. Cabri, A new copper-iron sulfide. *Econ. Geol.* **1967**, *62*, 910-925. https://doi.org/10.2113/gsecongeo.62.7.910.
[23] D. C. Harris, D. J. Vaughan, Two fibrous iron sulfides and valleriite from Cyprus with new data on valleriite. *Am. Mineral*. **1972**, *57*, 1037–1052.
[24] N. I. Organova, Crystallochemistry of modulated and incommensurate structures in minerals. *Int. Geol. Rev.* **1986**, *28*, 802-814. https://doi.org/10.1080/00206818609466322.
[25] R. Li, L. Cui, Investigations on valleriite from Western China: Crystal chemistry and separation properties. *Int. J. Miner. Process.* **1994**, *41*, 271-283. https://doi.org/10.1016/0301-7516(94)90033-7.
[26] F. B. Waanders, H. Pollak, Mössbauer spectroscopy to characterize iron sulphides. *South Afr. J. Sci*. **1999**, *95*, 387-390.

[27] A. Mücke, Review on mackinawite and valleriite: Formulae, localities, associations and intergrowths of the minerals, mode of formation and optical features in reflected light. *J. Earth Sci. Clim. Change* **2017**, *8*, 1000419. https://doi.org/10.4172/2157-7617.1000419.
[28] D. A. Dodin, *Metallogeniya Taimyro-Noril'skogo regiona (Metallogeny of Taimyr-Noril'sk region*), Nauka, St.-Petersburg, Russia **2002** (in Russian).
[29] Yu. V. Laptev, V. S. Shevchenko, F. Kh. Urakaev, Sulphidation of valleriite in SO_2 solutions. *Hydrometallurgy* **2009**, *98*, 201–205. https://doi.org/10.1016/j.hydromet.2009.04.018.
[30] A. E. Hughes, G. A. Kakos, T. W. Turney, T. B. Williams, Synthesis and structure of valleriite, a layered metal hydroxide/sulfide composite. *J. Solid State Chem*. **1993**, *104*, 422-436. https://doi.org/10.1006/jssc.1993.1178.
[31] D. C. Harris, L. J. Cabri, J. M. Stewart, A "valleriite-type" mineral from Noril'sk, Western Siberia. *Am. Mineral*. **1970**, *55*, 2110-2114.
[32] I. V. Pekov, E. V. Sereda, V. O. Yapaskurt, Y. S. Polekhovsky, S. N. Britvin, N. V. Chukanov, Ferrovalleriite, $2(Fe,Cu)S{\cdot}1.5Fe(OH)_2$: Validation as a mineral species and new data. *Geol. Ore Deposits* **2013**, *55*, 637-647. https://doi.org/10.1134/S1075701513080102.
[33] E. H. Nickel, D. R. Hudson, The replacement of chrome spinel by chromian valleriite in sulphide-bearing ultramafic rocks in Western Australia. *Contrib. Mineral. Petrol*. **1976**, *55*, 265-277. https://doi.org/10.1007/BF00371337.
[34] I. V. Pekov, V. O. Yapaskurt, Y. S. Polekhovsky, M. F. Vigasina, O. I. Siidra, Ekplexite $(Nb,Mo)S_2{\cdot}(Mg_{1-x}Al_x)(OH)_{2+x}$, kaskasite $(Mo,Nb)S_2{\cdot}(Mg_{1-x}Al_x)(OH)_{2+x}$ and manganokaskasite $(Mo,Nb)S_2{\cdot}(Mn_{1-x}Al_x)(OH)_{2+x}$, three new valleriite-group mineral species from the Khibiny alkaline complex, Kola Peninsula, Russia. *Mineral. Mag*. **2014**, *78*, 663–679. https://doi.org/10.1180/minmag.2014.078.3.14.
[35] N. I. Chistyakova, T. V. Gubaidulina, V. S. Rusakov, Mössbauer investigations of natural and synthetic tochilinite and valleriite. *Czech. J. Phys*. **2006**, *56*, E123–E131. https://doi.org/10.1007/s10582-006-0478-7.
[36] T. V. Gubaidulina, N. I. Chistyakova, V. S. Rusakov, Mössbauer study of layered iron hydroxysulfides: Tochilinite and valleriite. *Bull. Russ. Acad. Sci. Phys*. **2007**, *71*, 1269–1272. https://doi.org/10.3103/S106287380709016X.
[37] N. I. Chistyakova, V. S. Rusakov, T. V. Gubaidulina, A. M. Gapochka, A. Yu. Bychkov, Mössbauer investigations of synthetic valleriite. *Hyperfine Interact*. **2012**, *208*, 99–104. https://doi.org/10.1007/s10751-011-0474-6.
[38] Y. L. Mikhlin, A. S. Romanchenko, E. V. Tomashevich, M. N. Volochaev, Yu. V. Laptev, XPS and XANES study of layered mineral valleriite. *J. Struct. Chem*. **2017**, *58*, 1137–1143. https://doi.org/10.1134/S0022476617060105.
[39] Y. L. Mikhlin, M. N. Likhatski, O. A. Bayukov, Y. V. Knyazev, D. A. Velikanov, Y. V. Tomashevich, A. S. Romanchenko, S. A. Vorobyev, M. V. Volochaev, S. M. Zharkov, D. M. Meira, Valleriite, a natural two-dimensional composite: X ray absorption, photoelectron and Mössbauer spectroscopy and magnetic characterization. *ACS Omega* **2021**, *6*, 7533–7543. http://dx.doi.org/10.1021/acsomega.0c06052.
[40] M. Borgheresi, F. Di Benedetto, M. Romanelli, M. Reissner, W. Lottermoser, R. R. Gainov, R. R. Khassanov, G. Tippelt, A. Giaccherini, L. Sorace, G. Montegrossi, R. Wagner, G. Amthauer, Mössbauer Study of Bornite and Chemical Bonding in Fe-Bearing Sulphides. *Phys. Chem. Minerals* **2018**, *45*, 227-235. https://doi.org/10.1007/s00269-017-0911-4.

[41] K. Iiishi, T. Tomisaka, T. Kato, S. Takeno, Syntheses of valleriite. *Am. Mineral.* **1970**, *55*, 2107-2110.
[42] S. Takeno, G. H. Moh, Syntheses of selenian valleriite. *Mineral. Petrol*. **1994**, *50*, 209-218. https://doi.org/10.1007/BF01164606.
[43] X. F. Lu, N. Z. Wang, H. Wu, Y. P. Wu, D. Zhao, X. Z. Zeng, X. G. Luo, T. Wu, W. Bao, G. H. Zhang, F. Q. Huang, Q. Z. Huang, X. H. Chen, Coexistence of superconductivity and antiferromagnetism in $(Li_{0.8}Fe_{0.2})$OHFeSe. *Nature Mater*. **2015**, *14*, 325–329. https://doi.org/10.1038/nmat4155.
[44] U. Pachmayr, F. Nitsche, H. Luetkens, S. Kamusella, F. Brückner, R. Sarkar, H.-H. Klauss, D. Johrendt, Coexistence of 3d-ferromagnetism and superconductivity in $[(Li_{1-x}Fe_x)OH](Fe_{1-y}Li_y)Se$. *Angew. Chem. Int. Ed*. **2015**, *54*, 293–297. https://doi.org/10.1002/anie.201407756.
[45] X. Dong, K. Jin, D. Yuan, H. Zhou, J. Yuan, Y. Huang, W. Hua, J. Sun, P. Zheng, W. Hu, Y. Mao, M. Ma, G. Zhang, F. Zhou, Z. Zhao, $(Li_{0.84}Fe_{0.16})OHFe_{0.98}Se$ superconductor: Ion-exchange synthesis of large single-crystal and highly two-dimensional electron properties. *Phys. Rev. B* **2015**, *92*, 064515. https://doi.org/10.1103/PhysRevB.92.064515.
[46] D. N. Woodruff, F. Schild, C. V. Topping, S. J. Cassidy, J. N. Blandy, S. J. Blundell, A. L. Thompson, S. J. Clarke, The parent Li(OH)FeSe phase of lithium iron hydroxide selenide superconductors. *Inorg. Chem*. **2016**, *55*, 9886−9891. https://doi.org/10.1021/acs.inorgchem.6b01734.
[47] G. B. Hu, N. Z. Wang, M. Z. Shi, F. B. Meng, C. Shang, L. K. Ma, X. G. Luo, X. H. Chen, Superconductivity in solid-state synthesized (Li, Fe)OHFeSe by tuning Fe vacancies in FeSe layer. *Phys. Rev. Mater*. **2019**, *3*, 064802. https://doi.org/10.1103/PhysRevMaterials.3.064802.
[48] G. Hu, M. Shi, W. Wang, C. Zhu, Z. Sun, J. Cui, W. Zhuo, F. Yu, X. Luo, X. Chen, Superconductivity at 40 K in lithiation-processed $[(Fe,Al)(OH)_2][FeSe]_{1.2}$ with a layered structure. *Inorg. Chem*. **2021**, *60*, 3902−3908. https://dx.doi.org/10.1021/acs.inorgchem.0c03686
[49] U. Pachmayr, D. Johrendt, [(Li0.8Fe0.2)OH]FeS and the ferromagnetic superconductors [(Li0.8Fe0.2)OH]Fe(S1-*x*Se*x*). *Chem. Commun.* **2015**, *51*, 4689-4692. https://doi.org/10.1039/C5CC00038F.
[50] X. Zhou, C. Eckberg, B. Wilfong, S.-C. Liou, H. K. Vivanco, J. Paglione, E. E. Rodriguez, Superconductivity and magnetism in iron sulfides intercalated by metal hydroxides. *Chem. Sci*. **2017**, *8*, 3781–3788. https://doi.org/10.1039/c6sc05268a.
[51] A. Krzton-Maziopa, Intercalated iron chalcogenides: Phase separation phenomena and superconducting properties. *Front. Chem*. **2021**, *9*, 640361. https://doi.org/10.3389/fchem.2021.640361.
[52] R. V. Borisov, O. V. Belousov, A. M. Zhizhaev, Synthesis of Pd, Pt and Pd–Pt nanoparticles on carbon nanotubes under hydrothermal autoclave conditions. *Russ. J. Inorg. Chem*. **2020**, *65*, 1623–1629. https://doi.org/10.1134/S0036023620100034.
[53] A. P. Grosvenor, B. A. Kobe, M. C. Biesinger, N. S. McIntyre, Investigation of multiplet splitting of Fe 2p XPS spectra and bonding in iron compounds. *Surf. Interface Anal.* **2004**, *36*, 1564-1574.https://doi.org/10.1002/sia.1984.
[54] A. M. Sazonov, S. A. Silyanov, O. A. Bayukov, Y. V. Knyazev, Y. A. Zvyagina, P. A. Tishin, Composition and ligand microstructure of arsenopyrite from gold ore deposits of the

Yenisei Ridge (Eastern Siberia, Russia). *Minerals* **2019**, *9*, 737. https://doi.org/10.3390/min9120737.
[55] D. A. Velikanov, High-sensitivity measurements of the magnetic properties of materials at cryogenic temperatures. *Inorg. Mater. Appl. Res*. **2020**, *11*, 801–808. https://doi.org/10.1134/S2075113320040413.
[56] S. Goh, A. Buckley, R. Lamb, R. Rosenberg, D. Moran, The oxidation states of copper and iron in mineral sulfides, and the oxides formed on initial exposure of chalcopyrite and bornite to air. *Geochim. Cosmochim. Acta* **2006**, *70*, 2210–2228. https://doi.org/10.1016/j.gca.2006.02.007.
[57] Y. Mikhlin, V. Nasluzov, A. Ivaneeva, S. Vorobyev, M. Likhatski, A. Romanchenko, A. Krylov, S. Zharkov, D. M. Meira, Formation, evolution and characteristics of copper sulfide nanoparticles in the reactions of aqueous cupric and sulfide ions. *Mat. Chem. Phys*. **2020**, *255*, 123600. https://doi.org/10.1016/j.matchemphys.2020.123600.
[58] Y. Mikhlin, V. Nasluzov, A. Romanchenko, Y. Tomashevich, A. Shor, R. Felix, Layered structure of the near-surface region of oxidized chalcopyrite ($CuFeS_2$): Hard X-ray photoelectron spectroscopy, X-ray absorption spectroscopy and DFT+U studies. *Phys. Chem. Chem. Phys*. **2017**, *19*, 2749 – 2759. https://doi.org/10.1039/C6CP07598C.
[59] V. Nasluzov, A. Shor, A. Romanchenko, Y. Tomashevich, Y. Mikhlin, DFT + U and low-temperature XPS studies of Fe-depleted chalcopyrite ($CuFeS_2$) surfaces: A focus on polysulfide species. *J. Phys. Chem. C* **2019**, *123*, 21031–21041. https://doi.org/10.1021/acs.jpcc.9b06127.
[60] Y. Mikhlin, A. Romanchenko, Y. Tomashevich, Surface and interface analysis of iron sulfides in aqueous media using X-ray photoelectron spectroscopy of fast-frozen dispersions. *Appl. Surf. Sci*. **2021**, *549*, 149261. https://doi.org/10.1016/j.apsusc.2021.149261.
[61] M. Vos, S. W. King, B. L. French, Measurement of the band gap by reflection electron energy loss spectroscopy. *J. Electron Spectrosc. Rel. Phenom.* **2016**, *212*, 74–80. http://dx.doi.org/10.1016/j.elspec.2016.08.001.
[62] C. Richter, B. A. van der Pluijm, Separation of paramagnetic and ferrimagnetic susceptibilities using low temperature magnetic susceptibilities and comparison with high field methods. *Phys. Earth Planet. Inter*. **1994**, *83*, 113—123. https://doi.org/10.1016/0031-9201(94)90084-1.
[63] D. Peddis, D. Rinaldi, G. Ennas, A. Scano, E. Agostinelli, D. Fiorani, Superparamagnetic blocking and superspin-glass freezing in ultra small δ-($Fe_{0.67}Mn_{0.33}$)OOH particles. *Phys. Chem. Chem. Phys*. **2012**, *14*, 3162–3169. https://doi.org/10.1039/C2CP22473A.
[64] J. L. Dormann, R. Cherkaoui, L. Spinu, M. Noguès, F. Lucari, F. D'Orazio, D. Fiorani, A. Garcia, E. Tronc, J. P. Jovilet, From pure superparamagnetic regime to glass collective state of magnetic moments in γ-Fe_2O_3 nanoparticle assemblies. *J. Magn. Magn. Mater.* **1998**, *187*, L139-L144. https://doi.org/10.1016/S0304-8853(98)00135-8
[65] J. Navrátil, P. Levinský, J. Hejtmánek, M. Pashchenko, K. Knížek, L. Kubícková, T. Kmjec, C. Drašar, Peculiar magnetic and transport properties of $CuFeS_2$: Defects play a key role. *J. Phys. Chem. C* **2020**, *124*, 20773−20783. https://dx.doi.org/10.1021/acs.jpcc.0c06490.
[66] X. Zhang, Q.-H. Tan, J.-B. Wu, W. Shi, P.-H. Tan, Review on the Raman spectroscopy of different types of layered materials. *Nanoscale* **2016**, *8, 6435–6450.* https://doi.org/10.1039/c5nr07205k.
[67] https://rruff.info/valleriite/names/asc/R080119.

[68] https://rruff.info/chalcopyrite/names/asc/R050018.
[69] G. K. Parker, R. Woods, G. A. Hope, Raman investigation of chalcopyrite oxidation. *Colloids Surf. Physicochem. Eng. Asp.* **2008**, *318*, 160–168. https://doi.org/10.1016/j.colsurfa.2007.12.030.
[70] S.N. White, Laser Raman spectroscopy as a technique for identification of seafloor hydrothermal and cold seep minerals. *Chem. Geol.* **2009**, *259*, 240–252. https://doi.org/10.1016/j.chemgeo.2008.11.008.
[71] F. W. Ohrendorf, H. Haeuseler, Lattice dynamics of chalcopyrite type compounds. Part I. Vibrational frequencies. *Cryst. Res. Technol.* **1999**, *34*, 339–349. https://doi.org/10.1002/(SICI)1521-4079(199903)34:3%3C339::AID-CRAT339%3E3.0.CO;2-E
[72] M. Kosmulski, Isoelectric points and points of zero charge of metal (hydr)oxides: 50 years after Parks' review. *Adv. Colloid Interf. Sci.* **2016**, *238*, 1–61. https://doi.org/10.1016/j.cis.2016.10.005.
[73] B. Bhattacharyya, A. Pandey, $CuFeS_2$ quantum dots and highly luminescent $CuFeS_2$ based core/shell structures: Synthesis, tunability, and photophysics. *J. Am. Chem. Soc*. **2016**, *138*, 10207-10213. https://doi.org/10.1021/jacs.6b04981.
[74] G. Gabka, P. Bujak, A. Ostrowski, W. Tomaszewski, W. Lisowski, J. W. Sobczak, A. Pron, Cu-Fe-S nanocrystals exhibiting tunable localized surface plasmon resonance in the visible to NIR spectral ranges. *Inorg. Chem*. **2016**, *55*, 6660−6669. https://doi.org/10.1021/acs.inorgchem.6b00912.
[75] S. Ghosh, T. Avellini, A. Petrelli, I. Kriegel, R. Gaspari, G. Almeida, G. Bertoni, A. Cavalli, F. Scotognella, T. Pellegrino, L. Manna, Colloidal $CuFeS_2$ nanocrystals: intermediate Fe d-band leads to high photothermal conversion efficiency. *Chem. Mater*. **2016**, *28*, 4848-4858. https://doi.org/10.1021/acs.chemmater.6b02192.
[76] R. Gaspari, G. Della Valle, S. Ghosh, I. Kriegel, F. Scotognella, A. Cavalli, L. Manna, Quasi-static resonances in the visible Spectrum from all-dielectric intermediate band semiconductor nanocrystals. *Nano Lett*. **2017**, *17*, 7691−7695. https://doi.org10.1021/acs.nanolett.7b03787.
[77] S. Lee, S. Ghosh, C. E. Hoyer, H. Liu, X. Li, V. C. Holmberg, Iron-content-dependent, quasi-static dielectric resonances and oxidative transitions in bornite and chalcopyrite copper iron sulfide nanocrystals. *Chem. Mater*. **2021**, *33*, 1821–1831. https://doi.org/10.1021/acs.chemmater.0c04798.
[78] A. Agrawal, S. H. Cho, O. Zandi, S. Ghosh, R. W. Johns, D. J. Milliron, Localized surface plasmon resonance in semiconductor nanocrystals. *Chem. Rev*. **2018**, *118*, 3121−3207. https://doi.org/10.1021/acs.chemrev.7b00613.
[79] W. van der Stam, S. Gudjonsdottir, W. H. Evers, A. J. Houtepen, Switching between plasmonic and fluorescent copper sulfide nanocrystals. *J. Am. Chem. Soc*. **2017**, *139*, 13208−13217. https://doi.org/10.1021/jacs.7b07788.
[80] J. Tauc, Optical properties and electronic structure of amorphous Ge and Si. *Mater. Res. Bull*. **1968**, *3*, 37-46. https://doi.org/10.1016/0025-5408(68)90023-8.